CHEMIJA. 2019. Vol. 30. No. 2. P. 60–68

N-doped carbon material modified with cobalt nanoparticles as catalyst for oxygen reduction

Raminta Stagniūnaitė[1],

Virginija Kepenienė[1],

Zita Sukackienė[1],

Aldona Balčiūnaitė[1],

Gediminas Niaura[1],

Audrius Drabavičius[1],

Mindaugas Andrulevičius[2],

Ivar Kruusenberg[3],

Katlin Kaare[3],

Aleksandrs Volperts[4],

Galina Dobele[4],

Aivars Zhurinsh[4],

Loreta Tamašauskaitė-Tamašiūnaitė[1*],

Eugenijus Norkus[1]

[1] *Center for Physical Sciences and Technology,*
231 Savanorių Avenue,
02300 Vilnius, Lithuania

[2] *Institute of Materials Science of Kaunas,*
University of Technology,
59 Baršausko Street,
50131 Kaunas, Lithuania

[3] *Institute of Chemistry,*
University of Tartu,
14a Ravila Street,
50411 Tartu, Estonia

[4] *Latvian State Institute of Wood Chemistry,*
27 Dzerbenes Street,
1006 Riga, Latvia

In the present study, carbon-derived material from pulping residues, such as black liquor, was doped with a cheap nitrogen precursor, dicyandiamide, and after that modified with cobalt nanoparticles using electroless metal plating. The morphology, structure and composition of the synthesised catalyst was characterised using TEM, XPS, Raman Spectroscopy and ICP-OES, whereas the activity of the prepared catalyst was evaluated for the electro-reduction of oxygen in an alkaline medium by employing the rotating disk electrode method.

It has been determined that modifying of N-doped carbon material with cobalt nanoparticles results in enhanced activity for the oxygen electro-reduction as compared with that of pure N-doped carbon material.

Keywords: N-doped carbon, cobalt, nanoparticles, oxygen reduction

[*] Corresponding author. Email: loreta.tamasauskaite@ftmc.lt

INTRODUCTION

The oxygen reduction reaction (ORR) plays a significant role in the performance of numerous energy-conversion devices, including low-temperature fuel cells, metal-air batteries and certain electrolyzers [1]. Due to the sluggish reaction kinetics of the ORR at the cathode, the overall energy conversion efficiency of these technologies has been seriously limited [2]. Among the catalysts for ORR, Pt-based catalysts are regarded as the most active ones [3], whereas their application is limited due to the high price and limited resources of Pt. In order to obtain low-cost, high efficient and great performance catalysts for accelerating electrochemical oxygen reduction, various kinds of materials, including metal oxides, nitrides, oxynitrides, carbonitrides, metal chalcogenides, carbon-based non-noble metal and metal-free catalysts, have been intensively studied [4]. In addition, carbon-based metal-free catalysts are among the most promising non-precious-metal catalysts for ORR owing to their good activity, corrosion resistance, low cost, high electronic conductivity, and excellent surface properties [4–7]. The fabricated N-doped carbon materials [6,9], 2D nitrogen-doped hierarchically porous carbon [10], N and P co-functionalised three-dimensional porous carbon networks [11], N, S-codoped porous exfoliated carbon nanosheets [12], N-doped carbon nanotubes (NCNTs) [13–15], nitrogen-doped carbide-derived carbon (N-CDC) catalysts [16, 17] and nitrogen-rich carbon dots decorated graphene oxide (N-Cdots/GO) hybrid [18] have been described as highly-efficient and stable electrocatalysts for the oxygen reduction reaction. Moreover, N-doped carbon catalysts show a high electrocatalytic activity for ORR in both acidic and alkaline media [10, 11]. Among many non-noble metal catalysts, metal/nitrogen/carbon composites, such as Fe-N-C-based materials [19–22], nitrogen-doped carbon nanotubes with encapsulated Fe nanoparticles [23], non-precious Fe/N/S-composited hierarchically porous carbon materials [24], cobalt- and iron-containing nitrogen doped carbide-derived carbon materials [25] and binary Fe, Cu-doped bamboo-like carbon nanotubes [26] are also a promising alternative to Pt.

Recently, a great attention is focusing on biomass-derived electrocatalysts for the oxygen reduction reaction [27]. In this study, the pulping residue, such as black liquor, was used for preparation of electrocatalysts as the carbon source. The obtained carbon-derived material was doped with nitrogen and then modified with cobalt nanoparticles (CoNPs). The activity of the prepared catalysts was investigated for the oxygen reduction reaction.

EXPERIMENTAL

Chemicals

$CoSO_4$, dicyandiamide (DCDA), NaOH, dimethylformamide (DMF) and morpholine borane (MB) were purchased from the Sigma-Aldrich and Alfa-Aesar Suppliers.

Preparation of N-doped carbon material and its modification with cobalt nanoparticles

For preparation of N-doped carbon material, at first, the black liquor dry content was determined. Afterwards the amount of NaOH in a ratio of 2 to 1 of dry matter or black liquor was added and the mixture was thoroughly mixed and activated for 2 h in the stream of argon at 700°C temperature. Activated carbon was demineralised with subsequent HCl and deionised water washing. After that activated carbon was mixed with DCDA in a proportion of 20 to 1 in dimethylformamide (DMF) and evaporated until dry in a rotary evaporator. The resulting mixture was doped in the stream of argon for 1 h at 800°C temperature. Then, the prepared N-doped carbon material was modified with CoNPs using the electroless metal plating method. Morpholine borane was used as a reducing agent. The electroless cobalt plating bath contained the following (M): $CoSO_4$ – 0.07 and MB – 0.06. The bath operated at the solution pH 7 and at 50°C temperature. The deposition time of CoNPs was 30 min. After that, the obtained catalysts were rinsed with deionized water and dried in an oven at 80°C temperature.

Characterisation of catalysts

The shape and size of catalyst particles were examined using a transmission electron microscope Tecnai G2 F20 X-TWIN equipped with an EDAX spectrometer with an r-TEM detector. For microscopic examinations, 10 mg of the sample were first sonicated in 1 ml of ethanol

for 1 h and then deposited on a Cu grid covered with a continuous carbon film.

The chemical composition of the samples was analysed by means of the X-Ray Photoelectron spectroscopy method employing a Thermo Scientific ESCALAB 250Xi spectrometer. Monochromatized Al Kα radiation ($h\nu$ = 1486.6 eV) was used for excitation of photoelectrons. The base pressure in the analytical chamber was better than 8×10^{-7} Pa. The hemispherical electron energy analyser was operating in the Fixed Analyser Transmission mode and 40 eV pass energy. The energy scale of the system was calibrated according to the Au $4f_{7/2}$, Ag $3d_{5/2}$ and Cu $2p_{3/2}$ peaks position. The original ESCALAB 250Xi Avantage software was used for the peak fitting procedure.

Raman spectra were recorded using an inVia Raman (Renishaw, UK) spectrometer equipped with a thermoelectrically cooled (–70°C) CCD camera and a microscope. The Raman spectra were excited with 532 nm radiation from a diode pumped solid state (DPSS) laser (Renishaw, UK). The 20x/0.40 NA objective lens and 1800 lines/mm grating were used to record the Raman spectra. The accumulation time was 40 s. To avoid damage of the sample, the laser power at the sample was restricted to 0.6 mW. The Raman frequencies were calibrated using the polystyrene standard. Parameters of the bands were determined by fitting the experimental spectra with Gaussian-Lorentzian shape components using the GRAMS/A1 8.0 (Thermo Scientific) software.

The amount of the deposited CoNPs on the surface of the N-doped carbon material was estimated from the ICP optical emission spectra recorded with an ICP optical emission spectrometer Optima 7000 DV (Perkin Elmer).

ELECTROCHEMICAL MEASUREMENTS

A three-electrode electrochemical cell was used for electrochemical measurements. The working electrode was a glassy carbon electrode modified with the synthesised catalysts. The Pt sheet was used as a counter electrode and Ag/AgCl as a reference electrode. The catalyst ink (4 mg ml^{-1}) was obtained according to the following steps: at first, 2 mg of the synthesised catalysts were dispersed ultrasonically for 2 h in 500 µl 2% polyvinylidenefluoride in a N-methyl-2-pyrrolydone solution. Then, 5 µl of the prepared suspension mixture was pipetted onto the polished surface of the glassy carbon electrode with a geometric area of 0.07 cm^2 and dried in an oven at 80°C temperature for 4 h. The Co loading was 79 µg cm^{-2}.

All electrochemical measurements were performed with a Metrohm Autolab potentiostat (PGSTAT100) using the Electrochemical Software Nova. Linear-sweep voltammograms (LSVs) were recorded on the investigated catalysts in the O_2-saturated 0.1 M NaOH solution employing the rotating disk electrode (RDE) method at a scan rate of 10 mV s^{-1}. The rotation rate was varied from 0 to 2000 rpm. The electrode potential is quoted versus the reversible hydrogen electrode (RHE). The presented current densities are normalised with respect to the geometric area of catalysts.

RESULTS AND DISCUSSION

In the present study, the pulping residue, such as black liquor, was used as the carbon source for the preparation of N-doped carbon material. Further, the obtained N-doped carbon material was modified with CoNPs using the electroless metal deposition method and morpholine borane as a reducing agent. Figure 1 presents the TEM images of the bare N-doped carbon (a) and that modified with CoNPs (b). The corresponding EDX spectra of the CoNPs modified N-doped carbon confirm the presence of cobalt in the prepared material (Fig. 1c). Moreover, Co nanoparticles in the sample of approximately 15–25 nm in size were estimated. The chemical composition of the N-doped carbon and that modified with CoNPs was determined using X-ray photoelectron spectroscopy (XPS). Composition analysis and possible chemical bonds detection were performed analysing high-resolution spectra of oxygen, nitrogen, carbon and cobalt. Figure 2 shows the deconvoluted XP C1s (a) and N1s (b) spectra of the N-doped carbon material. The C1s peak consists mostly of sp^2 hybridised carbon [28], whereas the N1s peak was fitted and two peaks can be identified: pyridinic-N (398.23 eV) and pyrrolic-N (400.5 eV). The overall nitrogen content on this catalyst material was 7.44%, but most of nitrogen was in a pyridinic form.

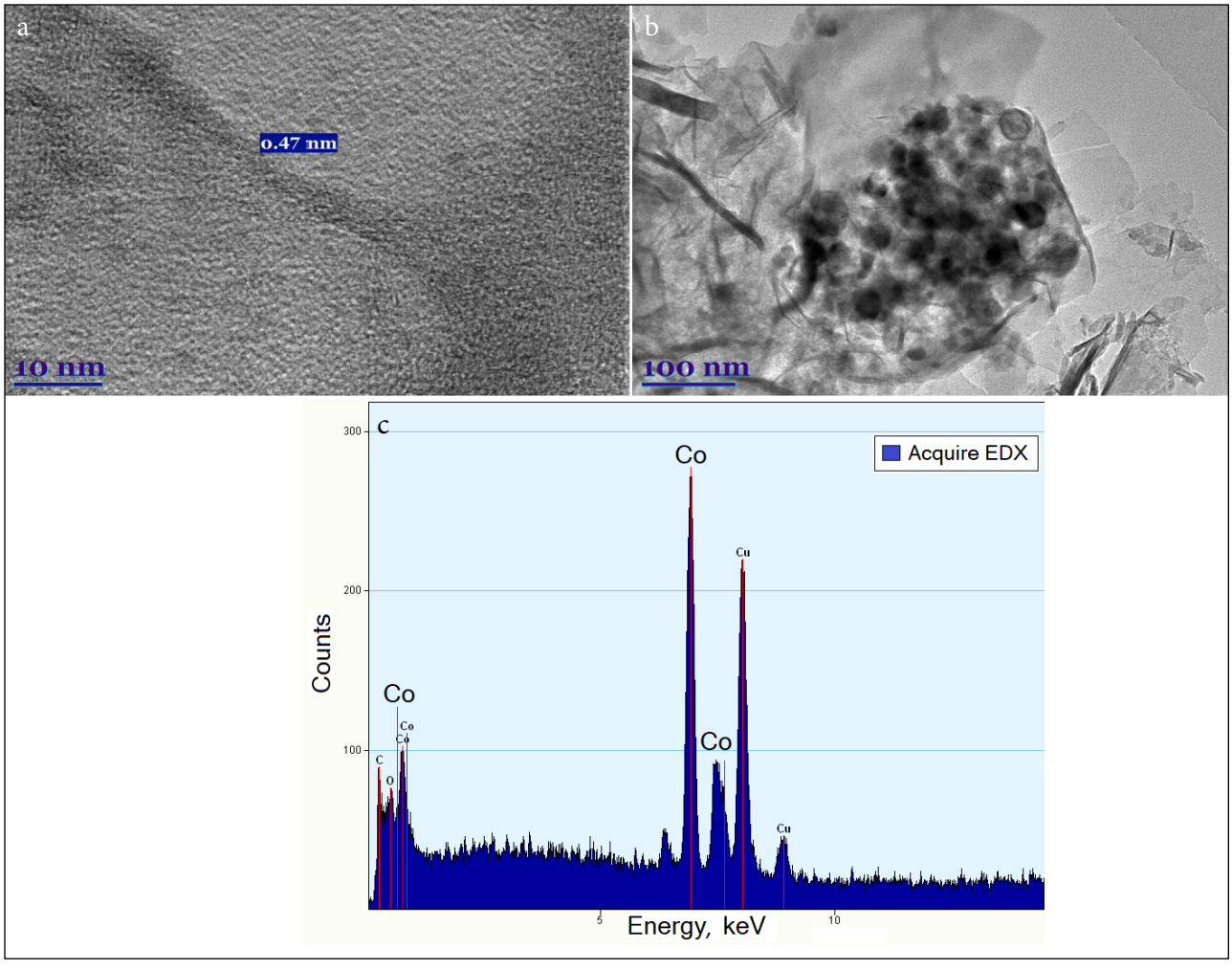

Fig. 1. TEM images of N-doped carbon (a) and that modified with CoNPs (b). (c) Represents the corresponding EDX spectra of N-doped carbon modified with CoNPs

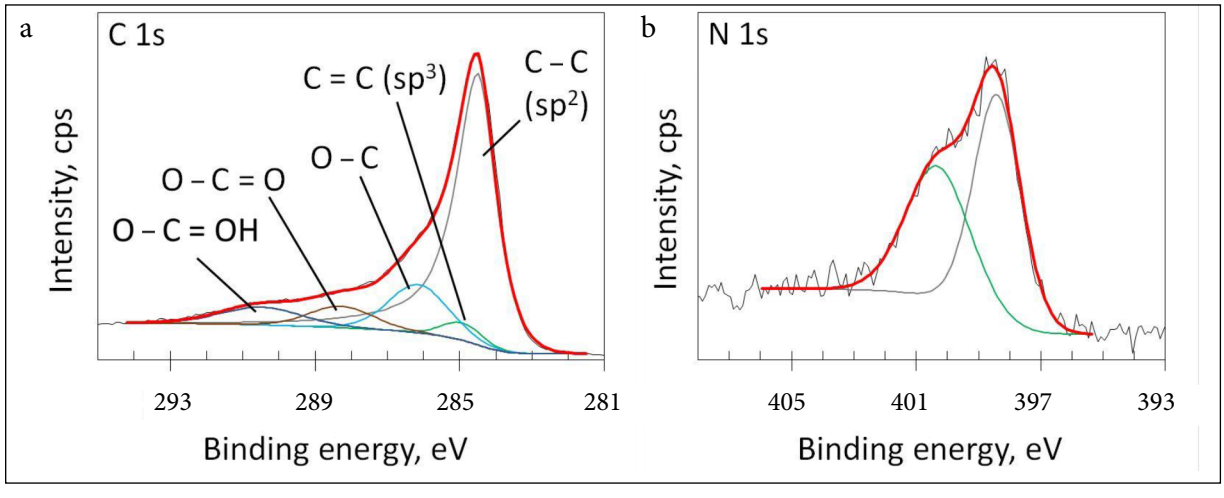

Fig. 2. Deconvoluted XP C1s (a) and N1s (b) spectra of N-doped carbon material

Figure 3a presents the XPS survey spectra for the N-doped carbon modified with CoNPs. The main peaks for carbon, oxygen, nitrogen and cobalt are indicated in this figure. The high intensity Co 2p peak doublet and lower intensity Co 2s, Co 3s and Co 3p peaks confidently indicate the presence

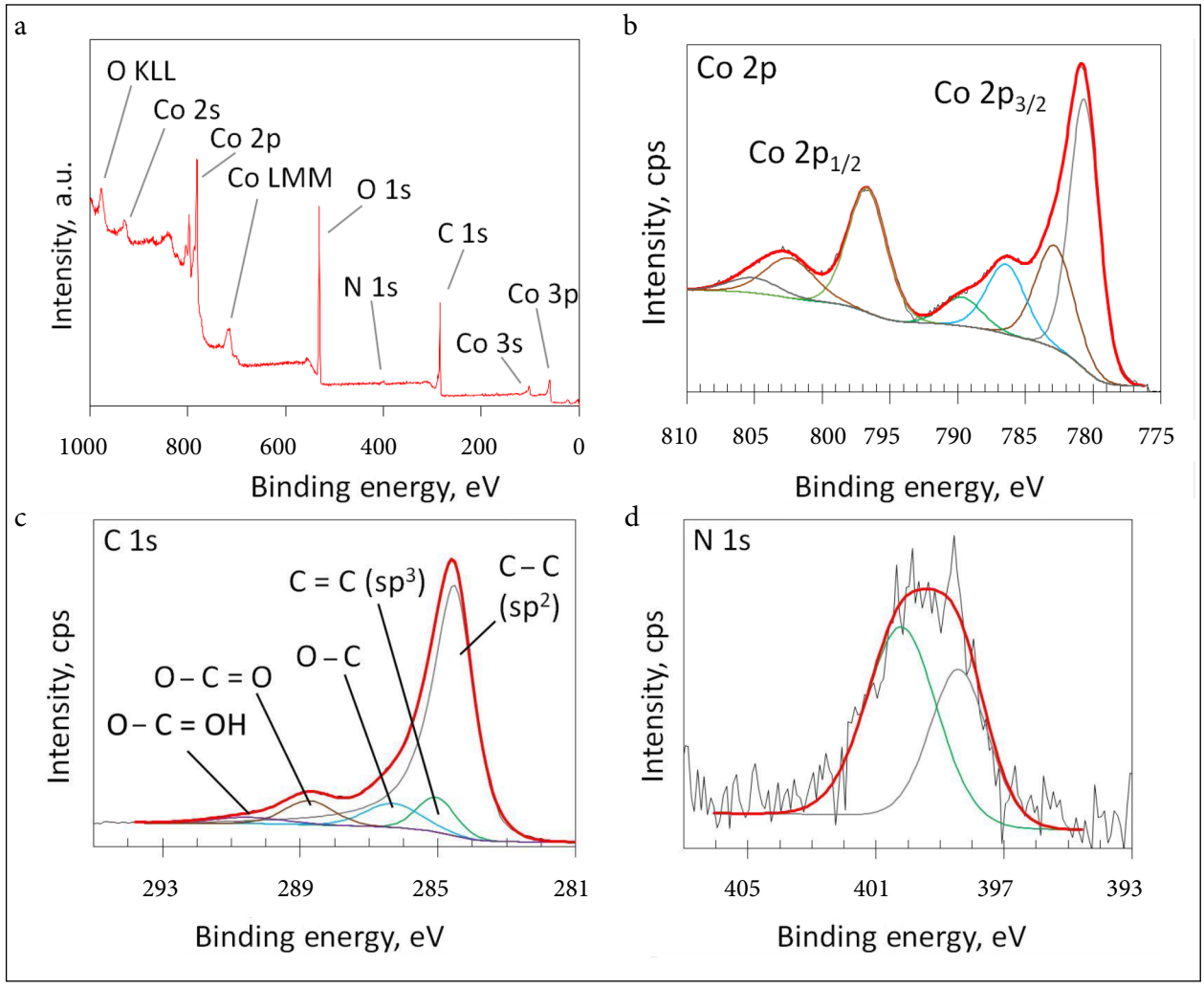

Fig. 3. XPS survey spectra (a), deconvoluted Co 2p (b), C1s (c) and N1s (d) spectra of N-doped carbon modified with CoNPs

of cobalt in this sample. It was determined that the cobalt content on this catalyst was 11.61 at.%, moreover, a relatively lower amount of nitrogen content of 2.97 at.% was in the N-doped carbon sample modified with CoNPs as compared with that of the pure N-doped carbon sample. The results of the deconvolution of Co 2p spectra for N-doped carbon modified with CoNPs (Fig. 3b) show typical two main peaks at 780.7 and 796.6 eV on a binding energy scale for Co 2p spin-orbit doublet Co $2p_{3/2}$ and Co $2p_{1/2}$, respectively. The position of the peak at 780.7 eV indicates that cobalt is in an oxidised state – according to binding energy values reported in literature for CoO (780.0, 780.3 and 780.9 eV) [29–31]. It is well known that cobalt monoxide CoO and cobalt oxide Co_2O_3 show similar binding energy values of the main Co $2p_{3/2}$ peak (CoO – 780.0 eV, Co_2O_3 – 779.6 eV) in [29], and (CoO – 780.3 eV, Co_2O_3 – 780.0 eV) in [30, 32]. Therefore, the most common method to distinguish between these two cobalt oxides is the analysis of the Co $2p_{1/2}$ peak area (calculating the intensity ratio of the main peak and 'shake up' satellite). The intensity ratio of the Co $2p_{1/2}$ satellite to its main peak is ~0.9 for CoO and ~0.3 for Co_3O_4 [30, 33, 34].

It has been reported that the intensity ratio of the Co 2p1/2 satellite to its main peak is ~0.9 for cubic CoO and ~0.3 for Co_3O_4 [30, 33, 34]], which is in agreement with the previous reported value of CoO.

Figure 4 compares the 532-nm excited Raman spectra of the studied samples: N-doped carbon (a) and that modified with CoNPs (b) materials in a frequency region of 400–3200 cm^{-1}. The dominant broad bands near 1598 and 1348 cm^{-1} belong to the characteristic G and D vibrations of sp^2 hybridised graphene layers [36–38]. The E_{2g}

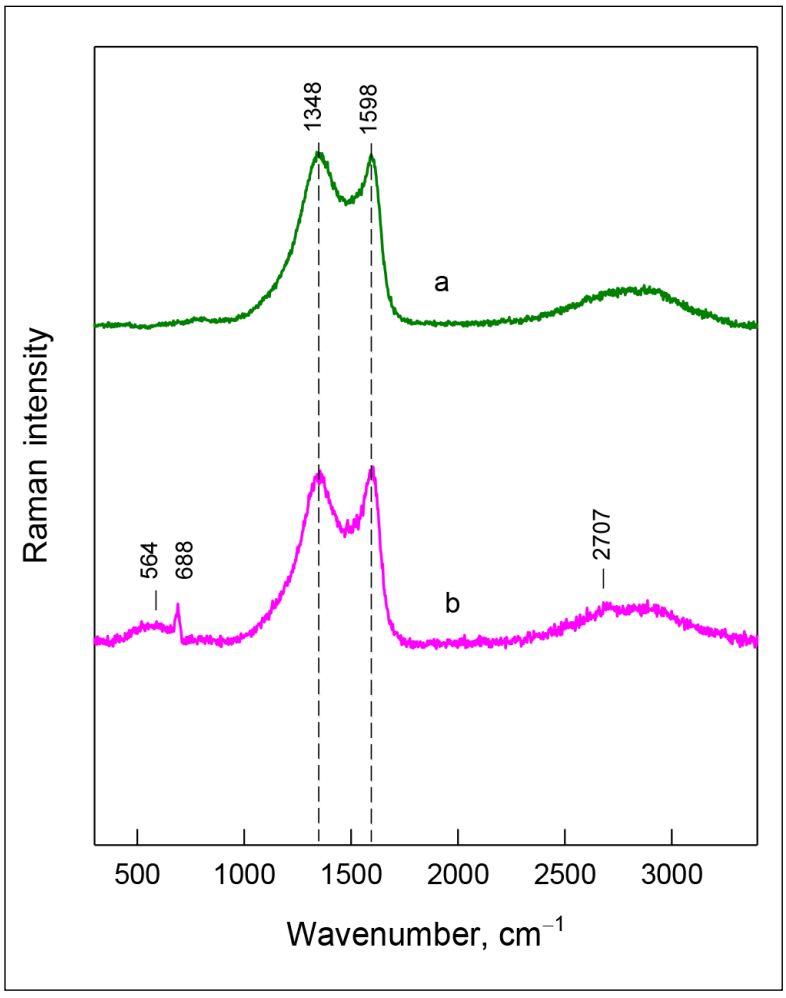

Fig. 4. Raman spectra of the N-doped carbon (a) and that modified with CoNPs (b). The excitation wavelength is 532 nm (0.6 mW)

symmetry G mode is associated with the in-plane relative motion of pairs of carbon atoms in sp^2 hybridization, while the A_{1g} symmetry D mode arises from the breathing vibrations of aromatic rings [36–38]. The G mode is always allowed, whereas presence of defects is required for the activation of the D mode. The 2D band (overtone of D mode) is not well-expressed and appears as a broad feature near 2707 cm^{-1}. Widths, peak positions and relative intensities of the above-discussed bands provide important information on the structure of carbon materials [36–41]. The intensity ratio of the D and G modes, I(D)/I(G), was used to probe the defect content in the sample [36–38]; the decrease in the intensity ratio reflects lowering of defectiveness of the sample. The studied samples exhibited a broad D and G band. The decomposition of experimental contours into the mixed Lorentzian-Gaussian form components revealed additional broad features near 1200 and 1540 cm^{-1}. The broad feature near 1500 cm^{-1} was previously associated with the D mode, which can serve as an indicator of carbon amorphisation [36, 39, 40]. Thus, our studied samples are highly disordered, containing the fraction of amorphous carbon. The analysis of the I(D)/I(G) ratio shows the highest value (1.02) for the N-doped carbon sample (spectrum (a)), while the lower ratio value (0.98) was found for the CoNPs-N-doped carbon sample (spectrum b).

The electrocatalytic oxygen reduction performance was investigated using the rotating disk electrode in an alkaline medium. Figure 5 shows the ORR poliarization curves for N-doped carbon (a) and that modified with CoNPs (b) in the 0.1 M NaOH solution with a scan rate of 10 mV s^{-1} over a range of rotation rates from 0 to 2000 rpm. The onset potential is equal to approximately 1.0 V for both the N-doped carbon and N-doped carbon material modified with CoNPs. Moreover, the current density increases with an increase in the rotation speed (Fig. 5a, b), which can be explained by a shortened diffusion distance at higher speeds. It should be noted that the current

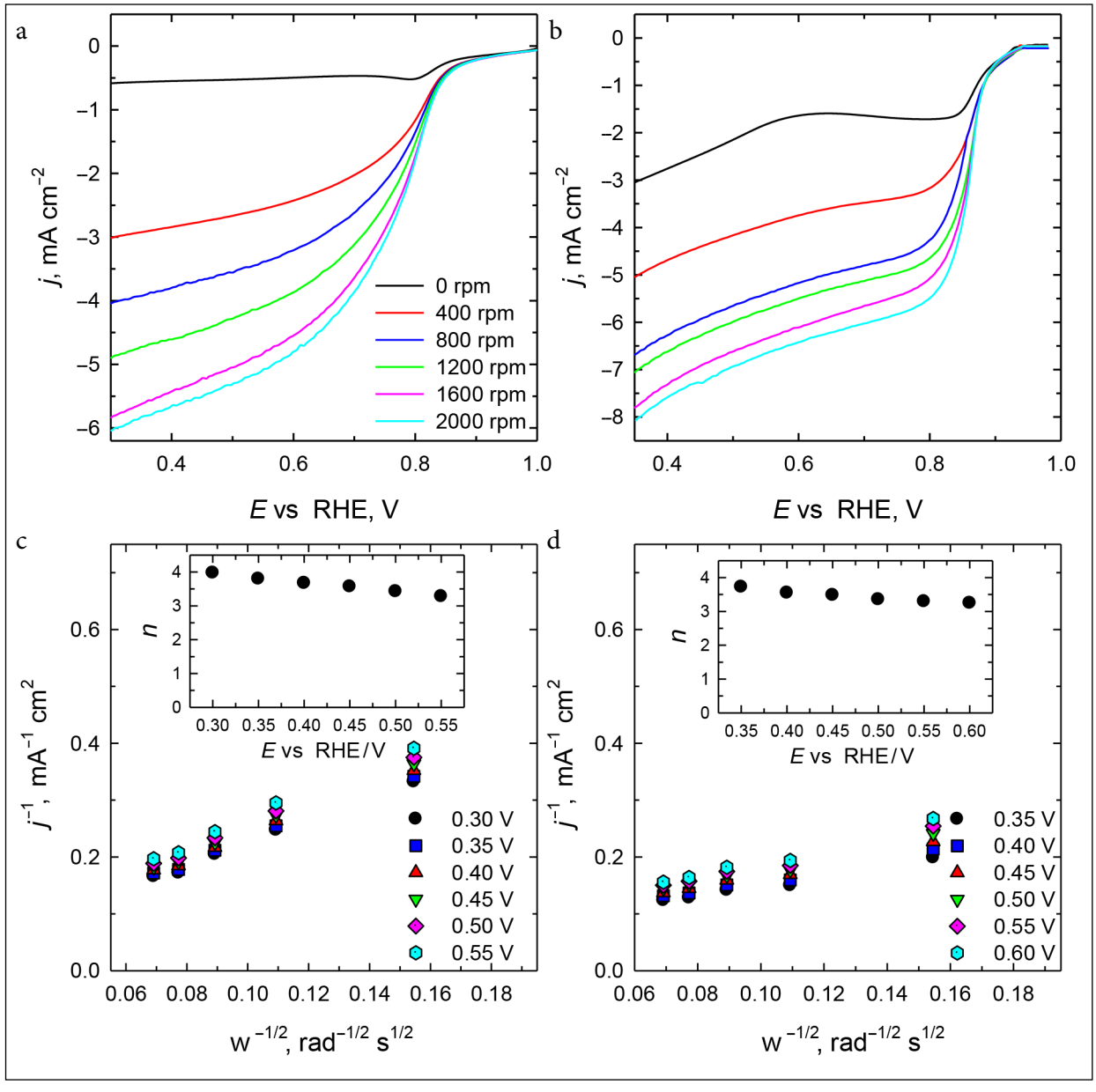

Fig. 5. LSV curves of N-doped carbon (a) and that modified with CoNPs (b) obtained at varied rotating rates in the O_2-saturated 0.1 M NaOH solution at a scan rate of 10 mV s^{-1}. (c) and (d) represent K–L plots derived from the RDE data. The insets in (c) and (d) show the potential dependence of *n*

densities are higher at the N-doped carbon material modified with CoNPs.

The number of electrons transferred per O_2 molecule (*n*) was calculated using the Koutecky–Levich (K–L) equation [41]

$$1/j = 1/j_k + 1/j_d = 1/\mathrm{B}\,\omega^{1/2} + 1/j_k;$$

$$\mathrm{B} = 0.62\,\mathrm{nFC_0(D_0)^{2/3}\nu^{-1/6}};\ j_k = \mathrm{nFkC_0}, \qquad (1)$$

where *j*, j_k and j_d are the experimentally measured current density, kinetic and diffusion-limiting current densities, respectively; *k* is the electrochemical rate constant for O_2 reduction, C_0 is the concentration of oxygen in the bulk (1.2×10^{-6}mol cm^{-3}) [42], F is the Faraday constant (96.485 C mol^{-1}), D_0 is the diffusion coefficient of O_2 (1.9×10^{-5} cm^2 s^{-1}) [37], ν is the kinematic viscosity of the solution (0.01 cm^2 s^{-1}) and ω is the rotation rate of the electrode (rad s^{-1}) [43]. The Koutecky–Levich (K–L) plots of the same catalysts at different potentials in a range of 0.3 up to 0.6 V are given in Fig. 5c and d. All the K–L plots show a good linearity, allowing the calculation of

the electron number transferred during the ORR process. The insets of Fig. 5c and d show the electron number n transferred at different potentials at the N-doped carbon material and that modified with CoNPs, respectively. In general, the K–L curves show a linear relationship between j^{-1} and $\omega^{-1/2}$ indicating the first-order dependence of the ORR kinetics at different potentials (0.3–0.6 V). Both materials showed a value of n close to 4 on all studied potentials (insets in Fig. 5c, d), meaning that these catalysts produce little to no hydrogen peroxide and are highly active for ORR.

The LSV curves recorded in the O_2-saturated NaOH solution at a RDE at 1600 rpm were compared to obtain further insight into the ORR catalytic activities of N-doped carbon and that modified with CoNPs (Fig. 6). It is clearly seen that the modification of N-doped carbon with cobalt nanoparticles (Fig. 6, a dashed line) significantly enhances its electrocatalytic activity for the oxygen electro-reduction reaction as compared with that of the pure N-doped carbon material (Fig. 6, a solid line).

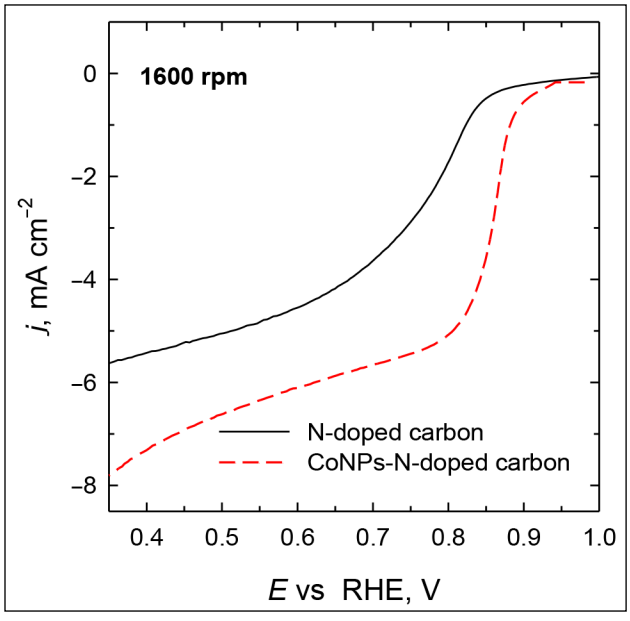

Fig. 6. LSV curves of N-doped carbon (a solid line) and that modified with CoNPs (a dashed line) obtained at 1600 rpm in the O_2-saturated 0.1 M NaOH solution at a scan rate of 10 mV s^{-1}

CONCLUSIONS

Novel non-precious electrocatalysts for ORR have been developed. N-doped carbon material has been derived using the pulping residue – black liquor as a carbon source. Further, the obtained N-doped carbon material has been modified with cobalt nanoparticles using the electroless metal deposition method and morpholine borane as a reducing agent.

It has been found that the N-doped carbon material shows a high electro-catalytic activity for the oxygen reduction reaction, whereas modifying of this material with cobalt nanoparticles results in enhanced activity for the oxygen electro-reduction as compared with that of the pure N-doped carbon material. The combination of metal nanoparticles with N-doped carbon materials opens up new possibilities for the design of cathode catalysts for oxygen reduction in the low-temperature fuel cells.

ACKNOWLEDGEMENTS

This research was funded by a grant (M-ERA.NET-1/2016) from the Research Council of Lithuania. The author's research was performed in cooperation with the University of Tartu (Estonia), Latvian State Institute of Wood Chemistry (Latvia) and Horizon Pulp & Paper Ltd (Estonia) under the M-ERA.NET 2 Project 'Wood-based Carbon Catalysts for Low-temperature Fuel Cells (WoBaCat)' (Reg. No. Project 3213).

Received 14 January 2019
Accepted 31 January 2019

References

1. L. Zeng, X. Cui, J. Shi, *Dalton Trans.*, **47**, 6069 (2018).
2. M. Borghei, J. Lehtonen, L. Liu, et al., *Adv. Mater.*, **30**, 1703691 (2018).
3. J. Stacy, Y. N. Regmi, B. Leonard, et al., *Renew. Sustain. Energy Rev.*, **69**, 401 (2017).
4. M. Shao, Q. Chang, J.-P. Dodelet, et al., *Chem. Rev.*, **116**, 3594 (2016).
5. H. C. Tao, Y. N. Gao, N. Talreja, et al., *J. Mater. Chem. A*, **5**, 7257 (2017).
6. L. Yang, S. Jiang, Y. Zhao, et al., *Angew. Chem. Int. Ed.*, **50**, 7132 (2011).
7. C. Raj, A. Samanta, S. Noh, et al., *J. Mater. Chem. A*, **4**, 11156 (2016).
8. J. Liu, P. Song, W. Xu., *Carbon*, **115**, 763 (2017).
9. Z.-Y. Sui, X. Li, Z.-Y. Sun, et al., *Carbon*, **126**, 111 (2018).
10. K. Wan, A.-D. Tan, Z.-P. Yu, et al., *Appl. Catal., B*, **209**, 447 (2017).
11. H. Jiang, Y. Wang, J. Hao, et al., *Carbon*, **122**, 64 (2017).

12. J.-T. Jin, X.-C. Qiao, F.-L. Cheng, et al., *Carbon*, **122**, 114 (2017).
13. M. Yang, D. Yang, H. Chen, et al., *J. Power Sources*, **279**, 85 (2015).
14. W. Y. Wong, W. R. W. Daud, A. B. Mohamad, et al., *Int. J. Hydrogen Energy*, **38**, 9421 (2013).
15. H. Deng, Q. Li, J. Liu, et al., *Carbon*, **112**, 219 (2017).
16. S. Ratso, I. Kruusenberg, M. Käärik, et al., *Carbon* **113**, 159 (2017).
17. S. Ratso, I. Kruusenberg, M. Käärik, et al., *J. Power Sources*, **375**, 233 (2018).
18. W.-J. Niu, R.-H. Zhu, Y.-H. Hua, et al., *Carbon*, **109**, 402 (2016).
19. M. M. Hossen, K. Artyushkova, P. Atanassov, et al., *J. Power Sources*, **375**, 214 (2018).
20. A. Mufundirwa, G. F. Harrington, B. Smid, et al., *J. Power Sources*, **375**, 244 (2018).
21. Y. Muna, M. J. Kim, S.-A. Park, et al., *Appl. Catal., B*, **222**, 191 (2018).
22. H. Tana, Y. Lia, X. Jiang, et al., *Nano Energy*, **36**, 286 (2017).
23. M. Rauf, R. Chen, Q. Wang, et al., *Carbon*, **125**, 605 (2017).
24. M. Wu, Q. Tang, F. Dong, et al., *J. Catal.*, **352**, 208 (2017).
25. S. Ratso, I. Kruusenberg, M. Käärik, et al., *Appl. Catal., B*, **219**, 276 (2017).
26. W. Fan, Z. Li, C. You, et al., *Nano Energy*, **37**, 187 (2017).
27. M. Borghei, J. Lehtonen, L. Liu, et al., *Adv. Mater.*, **30**, 1703691 (2018).
28. S. Pylypenko, S. Mukherjee, T. S. Olson, et al., *Electrochim. Acta*, **53**, 7875 (2008).
29. M. C. Biesinger, B. P. Payne, A. P. Grosvenor, et al., *Appl. Surf. Sci*., **257**, 2717 (2011).
30. W. Wang, G. Zhang, *J. Cryst. Growth*, **311**, 4275 (2009).
31. V. G. Bayev, J. A. Fedotova, J. V. Kasiuk, et al., *Appl. Surf. Sci*., **440**, 1252 (2018).
32. Y. E. Roginskaya, O. V. Morozova, E. N. Lubnin, et al., *Langmuir*, **13**, 4621 (1997).
33. J. Grimblot, J. P. Bonnelle, J. P. Beaufils, *J. Electron. Spectrosc. Relat. Phenom.*, **8**, 437 (1976).
34. H. M. Yang, J. Ouyang, A. D. Tang, *J. Phys. Chem. B*, **111**, 8006 (2007).
35. A. C. Ferrari, J. Robertson, *Phys. Rev. B*, **61**, 14095 (2000).
36. L. M. Malard, M. A. Pimenta, G. Dresselhaus, et al., *Phys. Rep*., **473**, 51 (2009).
37. R. Trusovas, G. Račiukaitis, G. Niaura, et al., *Adv. Optical Mater.*, **4**, 37 (2016).
38. R. Celiešiūtė, R. Trusovas, G. Niaura, et al., *Electrochim. Acta*, **132**, 265 (2014).
39. A. C. Ferrari, J. Robertson, *Phys. Rev. B*, **64**, 075414 (2011).
40. U. Paulus, T. Schmidt, H. Gasteiger, et al., *J. Electroanal. Chem*., **495**, 134 (2001).
41. A. J. Bard, L. R. Faulkner, *Electrochemical Methods: Fundamentals and Applications*, 2nd edn., Wiley, New York (2001).
42. R. E. Davis, G. L. Horvath, C. W. Tobias, *Electrochim. Acta*, **12**, 287 (1967).
43. D. R. Lide, *CRC Handbook of Chemistry and Physics*, 82nd edn., CRC Press, Boca Ration (2001).

**Raminta Stagniūnaitė, Virginija Kepenienė,
Zita Sukackienė, Aldona Balčiūnaitė, Gediminas Niaura,
Audrius Drabavičius, Mindaugas Andrulevičius,
Ivar Kruusenberg, Katlin Kaare, Aleksandrs Volperts,
Galina Dobele, Aivars Zhurinsh,
Loreta Tamašauskaitė-Tamašiūnaitė, Eugenijus Norkus**

KOBALTO NANODALELĖMIS MODIFIKUOTOS AZOTU DOPUOTOS ANGLIES KATALIZATORIAI DEGUONIES REDUKCIJAI

S a n t r a u k a

Deguonies redukcija buvo tiriama ant azotu dopuotos anglies ir kobalto nanodalelėmis modifikuotos azotu dopuotos anglies, naudojant sukamojo disko elektrodo metodą. Deguonies redukcija buvo tiriama O_2 prisotintame 0,1 M NaOH tirpale, skleidžiant elektrodo potencialą 10 mV s^{-1} greičiu ir keičiant elektrodo sukimosi greitį nuo 0 iki 2 000 apsisukimų/min. Nustatyta, kad azotu dopuotos anglies pagrindo modifikavimas kobalto nanodalelėmis pagerina katalizatoriaus elektrokatalizinį efektyvumą deguonies redukcijos reakcijai.